2009 American Control Conference
Hyatt Regency Riverfront, St. Louis, MO, USA
June 10-12, 2009

High-speed High-precision Control of Atomic Force Microscope by Surface Topography Learning Observer

Takayuki Shiraishi and Hiroshi Fujimoto

Abstract— **Purpose of this paper is realization of high-speed measurement atomic force microscope (AFM) from view point of the control technology without modification of the hardware. Almost commercial AFM, 3D-image is obtained from control input. High-speed imaging is possible if we can design feedback controller which achieves the high-bandwidth servo design. However, we know that it is restricted by bode integral theorem as resonance peak of the plant. For high-speed imaging, our research group proposed surface topography observer which based on the disturbance observer theory. we can locate the pole of the observer without considering of the resonance of the plant. Thus, we succeeded in high-speed imaging by our proposed observer. On the other hand, as the scanning speed of the X scanner becomes faster, the tracking error increases, because the feedback characteristic is same as conventional system. Not only the high-speed imaging but the suppression of the tracking error is important, because the tracking error express the contact force to the sample. Our research group proposed the tracking error suppression methods which are feedforward compensation. This paper describes the dual-directional type surface topography learning observer. This paper shows our proposed methods which are effective for the high-speed AFM by simulation and experimental results.**

I. INTRODUCTION

Atomic force microscope (AFM) is a very high-resolution type of scanning probe microscopes (STMs) which can measure nano-scale surface topography of a sample. AFM detects atomic force by various methods. Atomic force always exists between two atoms of a very close distance. Therefore, unlike STM which cannot measure the insulated sample, AFM does not have the restrictions to sample material. Briefly, AFM can measure any sample materials.

According to [1], problems of AFM are as following,
1) Ease of use: An expert operator is required, because operation of AFM is difficult
2) Repeatability/calibration: Re-adjustment is required at every exchange of the cantilever and the sample.
3) Measurement speed: Measurement speed of AFM is usually very slow.

In particular, the improvement of 3) is strongly desired in many industrial applications because low speed measurement causes undesirable environmental change in biological sample observation, and low working efficiency.

Most controllers for the high-speed measurement in the conventional AFM are the feedback control with analog implementation. However, many high-speed measurements for AFM are reported in recently. For instance, the active dumping method for suppressing the resonance peak of Z-piezo-electric actuator [2], feedforward compensation using the scanning information of the previous-line [3][4], Q control for maintaining the oscillating amplitude of the cantilever [5], and repetitive control [6] etc.

Our research group proposed some methods for high-speed AFM. For instance, surface topography observer [7] which estimates surface topography based on observer theory and the single directional type surface topography learning observer which utilized the pattern of the scanning route in contact mode [9].

This paper describes the dual-directional type surface topography learning observer. This paper shows our proposed methods are effective for the high-speed AFM by simulation and experimental results.

From the above background, the purpose of this paper is to achieve the high-speed measurement by control without sacrificing high measurement accuracy.

II. IDENTIFICATION OF THE SYSTEM

In this paper, we selected the contact-mode AFM as shown in Fig. 1. The bode diagram of the plant $P[z]$ is shown in Fig.3 which is measured by servo analyzer. In Fig. 4, the 2nd and 4th order of the discrete-time nominal plant $P_{n1}[z]$ and $P_{n2}[z]$ are drawn, respectively. These nominal plants are represented as follows. These discrete-time nominal plants are discretized by zero-order hold at sampling time $T_y = 40[us]$

$$P_{n1}(s) = \frac{9.296 \times 10^9}{s^2 + 5101s + 1.329 \times 10^9} \tag{1}$$

$$P_{n1}[z] = \frac{5.823(z + 0.929)}{z^2 - 0.210z + 0.815} \tag{2}$$

$$P_{n2}(s) = \frac{2.532 \times 10^{14}}{(s + 3.142 \times 10^4)(s^2 + 1810s + 5.116 \times 10^8)} \times \frac{s^2 + 2865s + 5.701 \times 10^8}{s^2 + 2149s + 1.283 \times 10^9} \tag{3}$$

$$P_{n2}[z] = \frac{1.801(z + 2.494)(z + 0.2142)}{(z - 0.2846)(z^2 - 1.193z + 0.9302)} \times \frac{(z^2 - 1.093z + 0.8919)}{(z^2 - 0.2652z + 0.9176)} \tag{4}$$

This work was not supported by any organization

T. Shiraishi is with Department of Electrical and Computer Engineering, Yokohama National University, Japan. shiraishi@hfl.dnj.ynu.ac.jp

H. Fujimoto is with Department of Electrical and Computer Engineering, Yokohama National University, Japan. hfuji@ynu.ac.jp

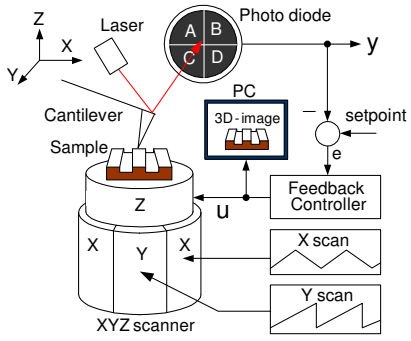

Fig. 1. Measurement principle of contact-mode AFM.

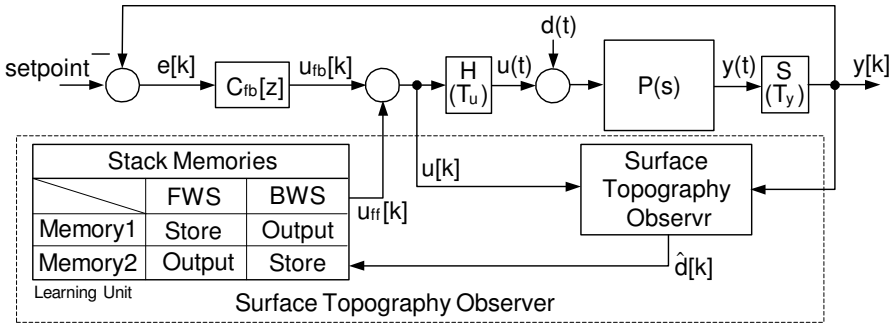

Fig. 2. Block diagram of control system.

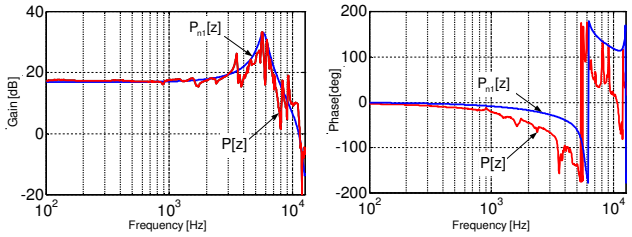

Fig. 3. Frequency responses of plant $P[z]$ and nominal plant $P_{n1}[z]$.

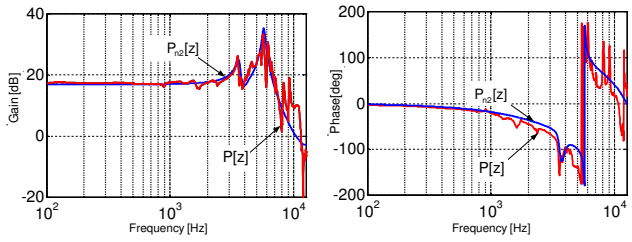

Fig. 4. Frequency responses of plant $P[z]$ and nominal plant $P_{n2}[z]$.

III. CONTROLLER DESIGN

In this section, controller design is presented. The control system of this paper is shown in Fig.2.

A. Feedback controller

The feedback controller $C_{fb}(s)$ is represented by

$$C_{fb}(s) = 0.005 \times \frac{s + 600\pi}{s} \times C_{notch}(s). \tag{5}$$

where, $C_{notch}(s)$ is the notch filter which is represented by

$$C_{notch}(s) = \prod_{r=1}^{3} \frac{s^2 + Q_r\omega_r s + \omega_r^2}{s^2 + Q_r A_r \omega_r s + \omega_r^2}. \tag{6}$$

$$\begin{bmatrix} Q_1 & A_1 & \omega_1 \\ Q_2 & A_2 & \omega_2 \\ Q_3 & A_3 & \omega_3 \end{bmatrix} = \begin{bmatrix} 0.30 & 0.04 & 43982.29 \\ 0.10 & 0.20 & 78539.81 \\ 0.10 & 0.35 & 5654.867 \end{bmatrix}$$

where, ω_r, Q_r and A_r are the notch frequency, the parameter of the notch depth and width, respectively. $C_{notch}(s)$ is descritized by prewarped tustin at the sampling time T_y. Fig. 4 shows the bode diagram of the open-loop characteristics $P[z]C_{fb}[z]$. In commercial AFM, the control input $u(t)$ is used to obtain the image of the sample surface topography $d(t)$. The transfer function from $d(t)$ to $u(t)$ can be derived as

$$T(s) = -\frac{u}{d} = \frac{C_{fb}(s)P(s)}{1 + C_{fb}(s)P(s)}. \tag{7}$$

From (7), if we can design the high-bandwidth servo controller $C_{fb}(s)$, control input can achieve the high-speed imaging. However, it is difficult to realize the high-speed imaging, because the plant usually has resonance peak.

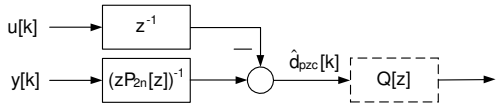

Fig. 5. Pole-zero cancel based STO.

B. Surface topography observer ; STO

In this subsection, the high-speed imaging method of the sample surface topography using observer is presented. The high-speed imaging by quosi-observer was reported in [10]. Author's group also proposed surface topography observer (STO) which is based on the disturbance observer theory. In this subsection, three types of STO are explained.

The surface topography d is the assumption that the input disturbance, output y is represented by

$$y[k] = P[z](u[k] + d[k]) + n[k]. \tag{8}$$

From (8), if $n[k] = 0$, the surface topography $d[k]$ is obtained by

$$d[k] = P[z]^{-1}y[k] - u[k]. \tag{9}$$

Thus, we can know that the surface topography d will be estimated from the output y, the control input u and the inverse system of the plant $P[z]^{-1}$.

1) pole-zero cancel type STO: The discrete-time plant $P[z]$ is decsritized by zero-order hold at sampling time T_y. It is known that the discrete-time system has unstable zeros when the relative degree of the continuous-time system more than three [14]. If we select the P_{n2}, we can design the stable inverse system of the plant, because the continuous time plant $P_{n2}(s)$ is 2nd order system. From (9), when the nominal

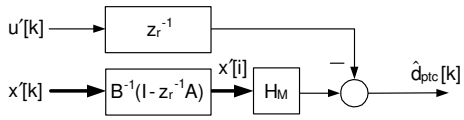

Fig. 6. Perfect tracking control based STO

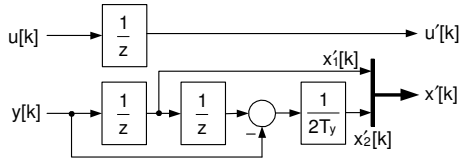

Fig. 7. Perfect tracking control based STO

plant and the plant are equal, the one-sample delayed surface topography is obtained by

$$\hat{d}_{pzc}[k] = \frac{1}{zP_{n2}[z]}y[k] - \frac{1}{z}u[k] = \frac{1}{z}d[k]. \quad (10)$$

where, $1/zP_{n2}[z]$ is the stable and proper system. This observer is called pole-zero cancel type surface topography observer (PZC-STO) in this paper. The zero of the plant $P[z]$ is -0.928 which is near the unstable zero. Thus, although $\hat{d}_{pzc}[k]$ is stable, it behavior will be easily oscillating.

2) Perfect tracking control method based STO: Perfect tracking control method (PTC) is one of the 2DOF control method which is usually applied to the precise positioning control system. When the nominal plant and the plant are equal, PTC can achieve the zero tracking error at the every sampling time T_r. Consider the continuous-time nth state equation is described by

$$\dot{\boldsymbol{x}}(t) = \boldsymbol{A}_c\boldsymbol{x}(t) + \boldsymbol{b}_c(u(t) + d(t)), \;\; y(t) = \boldsymbol{c}_c\boldsymbol{x}(t). \quad (11)$$

The discrete-time state space equation discretized by the shorter period T_u becomes

$$\boldsymbol{x}[k+1] = \boldsymbol{A}_s\boldsymbol{x}[k] + \boldsymbol{b}_s(u[k] + d[k]) \quad (12)$$
$$y[k] = \boldsymbol{c}_s\boldsymbol{x}[k]. \quad (13)$$

where, $x[k] = x(kT_u)$ and,

$$\boldsymbol{A}_s = e^{\boldsymbol{A}_c T_u}, \quad \boldsymbol{b}_s = \int_0^{T_u} e^{\boldsymbol{A}_c\tau}\boldsymbol{b}_c d\tau. \quad (14)$$

By calculating the state transition from $t = iT_y = kT_u$ to $t = (i+1)T_y = (k+n)T_u$, the discrete-time plant $P[z]$ can be represented by

$$\boldsymbol{x}[i+1] = \boldsymbol{A}\boldsymbol{x}[i] + \boldsymbol{B}(\boldsymbol{u}[i] + \boldsymbol{d}[i]) \quad (15)$$

where $\boldsymbol{x}[i] = \boldsymbol{x}(iT_y), z := e^{sT_y}$ and multirate input vector u is defined in the lifting form as

$$\boldsymbol{u}[i] : = [u_1[i], \cdots, u_n[i]]^T \quad (16)$$
$$= [u(kT_u), \cdots, u((k+n-1)T_u)]^T \quad (17)$$

and the coefficients are given by

$$\boldsymbol{A} = \boldsymbol{A_s^n}, \boldsymbol{c} = \boldsymbol{c_c} \quad (18)$$
$$\boldsymbol{B} = [\boldsymbol{A_s^{n-1}b_s}, \boldsymbol{A_s^{n-2}b_s}, \cdots, \boldsymbol{A_s b_s}] \quad (19)$$

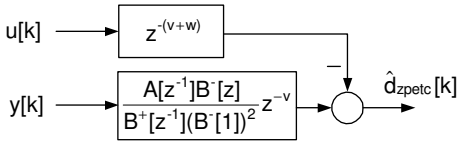

Fig. 8. ZPETC based STO

From (15), the transfer function from $\boldsymbol{x}[i+1]$ to the multirate input and the surface topography $(\boldsymbol{u}[i] + \boldsymbol{d}[i])$ can be derived as

$$\boldsymbol{u}[i] + \boldsymbol{d}[i] = \boldsymbol{B}^{-1}(\boldsymbol{I} - z_r^{-1}\boldsymbol{A})\boldsymbol{x}[i+1] \quad (20)$$
$$= \left[\begin{array}{c|c} \boldsymbol{O} & \boldsymbol{I} \\ \hline \boldsymbol{-B^{-1}A} & \boldsymbol{B^{-1}} \end{array}\right]\boldsymbol{x}[i+1]. \quad (21)$$

From the definition in (17), the nonsingular matrix $\boldsymbol{B}$ is assured for a controllable plant. Moreover, all poles of the transfer function are zero from (21). Hence, (21) is a stable inverse system. From (21), The surface topography $\boldsymbol{d}[i]$ is represented by

$$\hat{\boldsymbol{d}}[i] = \boldsymbol{B}^{-1}(\boldsymbol{I} - z_r^{-1}\boldsymbol{A})\boldsymbol{x}[i+1] - \boldsymbol{u}[i]. \quad (22)$$

It is impossible to get the future state space variables $\boldsymbol{x}[i+1]$, we estimate one sample delayed surface topography which is represented by

$$\hat{\boldsymbol{d}}[i]_{ptc} = {z_r}^{-1}\boldsymbol{B}^{-1}(\boldsymbol{I} - z_r^{-1}\boldsymbol{A})\boldsymbol{x}[i] - {z_r}^{-1}\boldsymbol{u}[i]. \quad (23)$$

The block diagram of the PTC-STO is shown in Fig. 6 which use the state variable. In this paper, the detectable state variable is the output y only ($y = x_1[k]$). The velocity of the cantilever is calculated by

$$x_2[k] \cong \frac{y[k-1] - y[k+1]}{2T_u}. \quad (24)$$

It is note that the $\hat{\boldsymbol{d}}_{ptc}[i]$ is calculated at sampling time $T_r(= nT_k)$, and is vector. we can obtain the $\hat{d}_{ptc}[k]$ which is the surface topography at sampling time T_k by multirate holder H_M as shown in Fig. 7.

3) Zero phase error tracking controller based STO [13]: The discrete-time transfer function of the plant is represented by

$$P[z^{-1}] = \frac{z^{-w}B[z^{-1}]}{A[z^{-1}]}. \quad (25)$$

where,

$$B[z^{-1}] = \acute{b}_0 + \acute{b}_1 z^{-1} + \cdots + \acute{b}_m z^{-m}, \; \acute{b}_0 \neq 0 \quad (26)$$
$$A[z^{-1}] = 1 + \acute{a}_1 z^{-1} + \cdots + \acute{a}_n z^{-n} \quad (27)$$
$$d = n - m \quad (28)$$

The poles of $A[z^{-1}]$ are stable. $B[z^{-1}]$ is divided into stable and unstable zeros part as follows.

$$B[z^{-1}] = B^-[z^{-1}]B^+[z^{-1}] \quad (29)$$

where, $B^-[z^{-1}]$ is the s-th order monic polynomial equation which include the unstable or limit of the stable zeros, and

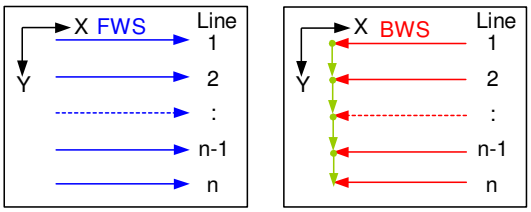

Fig. 9. Scan route of XY scanner.

$B^+[z^{-1}]$ is the $(m-v)th$ order monic polynomial equation which include the stable zeros. Then, ZPETC based inverted model of the plant is obtained by

$$P_{ZPEI} = \frac{A[z^{-1}]B^-[z]}{B^+[z^{-1}](B^-[1])^2}z^{-v}. \quad (30)$$

where, $B^-[z] = B^-[z^{-1}]z^v$. When (30) is applied to the following control system, it is inserted before the plant, and if $r[k+v+w]$ which is the future value of the reference input r in which the $[v+w]$ steps time forward is given, the zero phase error characteristic in which r to y have no phase lag under the nyquist frequencies [13].

From (9) and (30), we can design the STO which is based on ZPETI. The estimated surface topography is represented by

$$\hat{d}_{zpetc}[k] = P_{ZPEI}[z]y[k] - z^{-(v+w)}u[k] \quad (31)$$

$$= \frac{B^-[z^{-1}]B^-[z]}{(B^-[1])^2}z^{-(v+w)}d[k]. \quad (32)$$

The block diagram of ZPETC based STO is shown in Fig.8.

C. Feedforward controller

Although STO can achieve the high-speed estimation of the sample surface, the suppression of the tracking error is dependent on the feedback system. To suppress the tracking error, our research group proposed some kind of surface topography learning observers (STLO) [8] which is feedforward compensation.

$$u[k] = u_{fb}[k] + u_{ff}[k] \quad (33)$$

In this paper, we applied dual-directional type STLO (DD-STLO) to AFM.

1) Dual directional type STLO: Fig. 2 shows the block diagram of DD-STLO which has two stack memories and STO. The time chart of DD-STLO is shown in Fig. 10. In FWS, the estimated surface topography $\hat{d}$ is stored in memory1. Then, the memory2 outputs the feedforward input u_{ff}. In BWS, the estimated surface topography $\hat{d}$ is stored in memory2. Then the memory1 outputs the feedforward input u_{ff}. The control input $u[k]$ is given as $u[k] = u_{fb}[k]+u_{ff}[k]$ from Fig. 2.

2) Timing of feedforward: It is assumed that the estimated surface topography $\hat{d}[k]$ can be expressed only with surface topography $d[k]$ and dead time z^{-h}. Then, $\hat{d}[k]$ is obtained by $\hat{d}[k] = z^{-h}d[k]$. Thus, the surface topography is obtained by $d[k] = z^h\hat{d}[k]$ which is used to u_{ff}. In DD-STLO, we

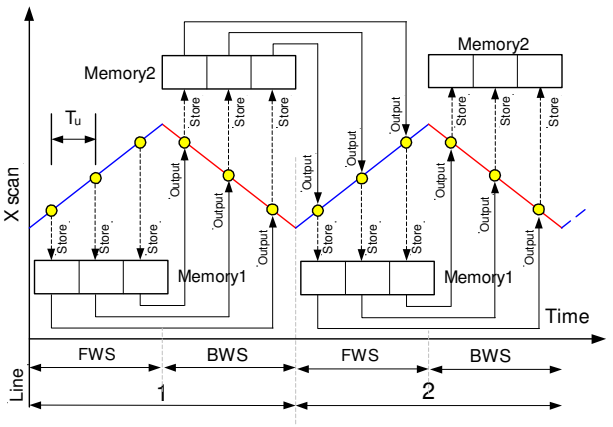

Fig. 10. Timing of learning and feedforward input of DD-STLO.

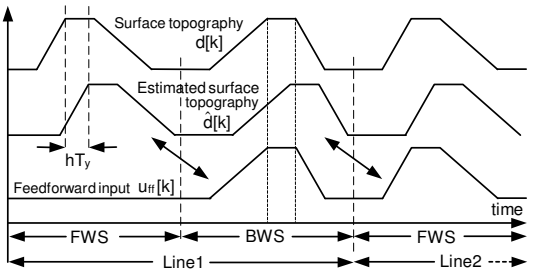

Fig. 11. Timing of learning and feedforward input of DD-STLO.

can know the $z^h\hat{d}[k]$ which is the future value from the stack memory. In order to correspond the timing of the feedforward input $u_{ff}[k]$ and surface topography $d[k]$, the delay component of z^{-h} is used. Then, the timing of $u_{ff}[k]$ and $d[k]$ will be corresponded as Fig.11.

The Table shows the delay time for feedforward input $u_{ff}[k]$ which is obtained from (10), (23) and (32) respectively.

IV. Simulation and Experimental Results

A. Simulation

Simulation results as shown in Fig. 12. The blue line is the surface topography , and the red line is the estimated surface topography of the sample. (a),(b), and (c) are PZC-STO, PTC-STO(ideal), and PTC-STO (using the central difference), respectively. From (a) and (b), It is known that PTC-STO can achieve the stable estimation with measurement noise.

B. Experimental results

Experimental results show Fig. 13 to Fig. 17. Fig.13 shows the frequency responses from the surface topography d to the

TABLE I
DELAY TIME OF THE FEEDFORWARD INPUT $u_{ff}[k]$

	PZC-STO	PTC-STO	ZPETC-STO
h	1	n	$v+w$

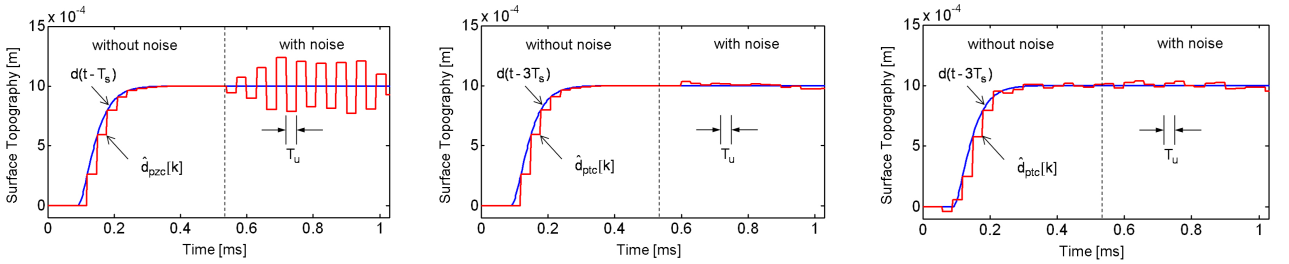

(a)PZC-STO $\hat{d}_{pzc}$ (b) PTC-STO $\hat{d}_{ptc}$(Ideal) (c) PTC-STO $\hat{d}_{ptc}$ (central difference)

Fig. 12. Simulation results: time responses of $\hat{d}[k]$.

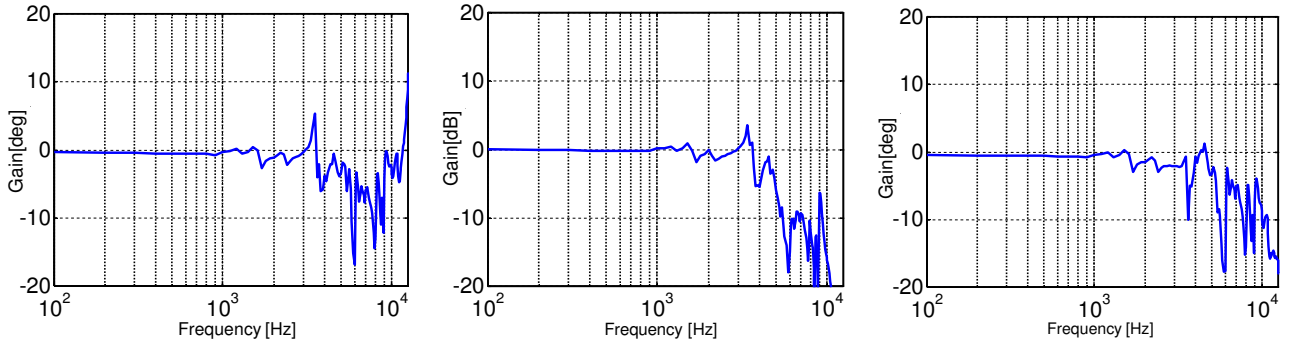

(a)PZC-STO (b)PTC-STO (c) ZPETC-STO

Fig. 13. Experimental results: frequency responses of $u_{ff}[k]/d[k]$.

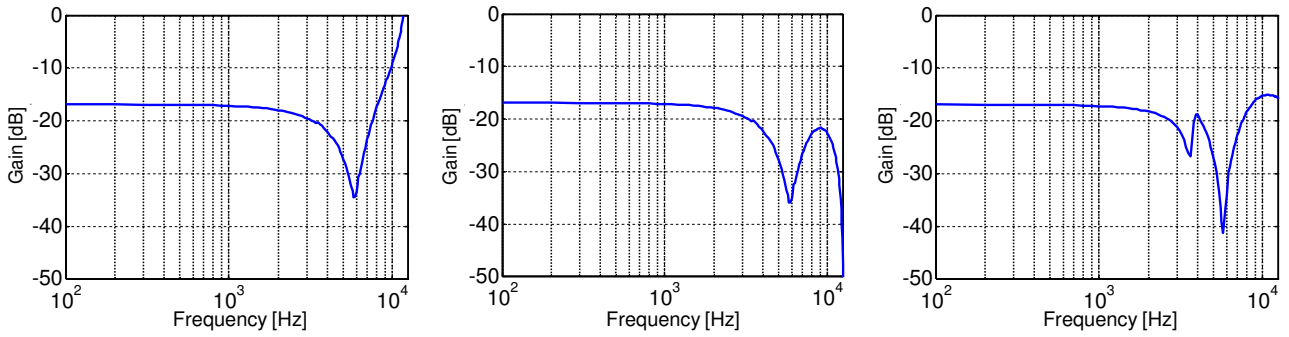

(a)PZC-STO (b)PTC-STO (c) ZPETC-STO

Fig. 14. Experimental results: frequency responses of $\hat{d}[k]/n[k]$.

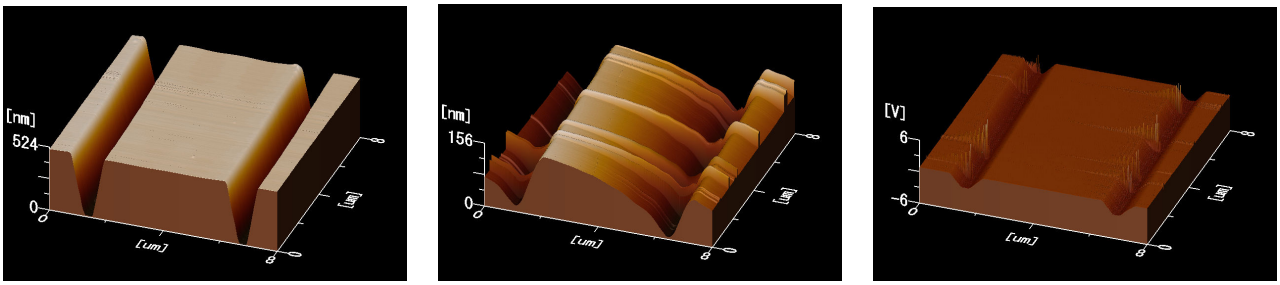

(a) Reference image u
Scan speed 7.32 μm/s, 684 s/image

(b) Conventional u
Scan speed 732 μm/s, 6.84 s/image

(c) PZC-STO $\hat{d}_{pzc}$
Scan speed 732 μm/s, 6.84 s/image

Fig. 15. Experimental results: 3D-images.

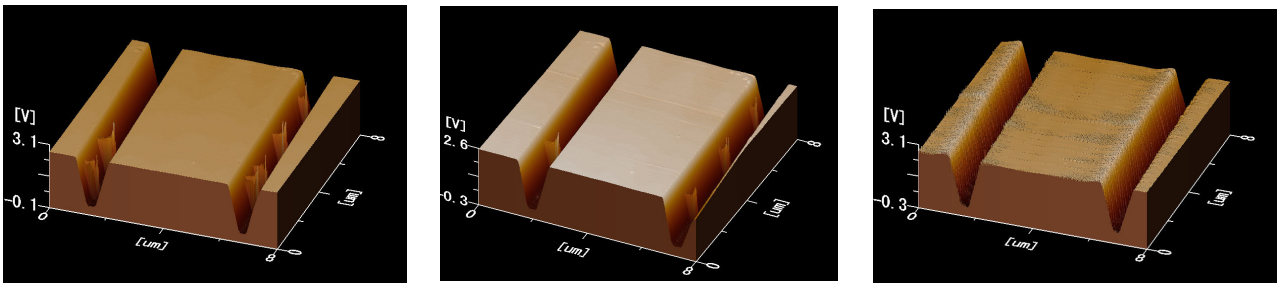

(a)PTC-STO $\hat{d}_{ptc}$
Scan speed 732 μm/s, 6.84 s/image

(b)ZPETC-STO $\hat{d}_{zpetc}$
Scan speed 732 μm/s, 6.84 s/image

(c)PTC-STO with DD-STLO
Scan speed 732 μm/s, 6.84 s/image

Fig. 16. Experimental results: 3D-images.

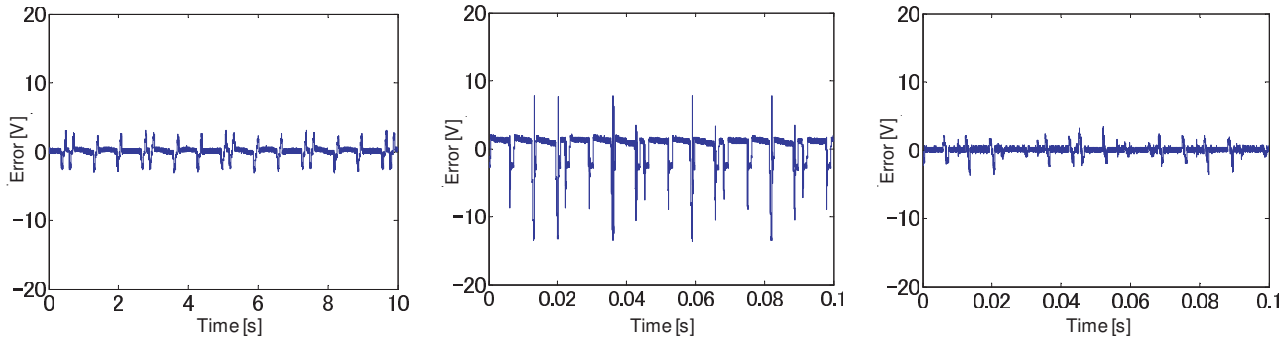

(a) without DD-STLO
Scan speed 7.32 μm/s, 684 s/image

(b)without DD-STLO
Scan speed 732 μm/s, 6.84 s/image

(c) with DD-STLO
Scan speed 732 μm/s, 6.84 s/image

Fig. 17. Experimental results: with and without DD-STLO.(Scan speed: 732 μm/s and 7.32 μm/s)

estimated surface topography $\hat{d}$. Fig.14 shows the frequency responses from noise to the estimated surface topography $\hat{d}$. Fig.15 shows the 3D-images of the surface topography. Fig.16 is also shows the 3D-images of the surface topography. From Fig.15 and Fig. 16, STO can achieve the high-speed imaging comparing (b) with others.

Fig.17 shows the tracking errors. The scan speed of (a) is very slow scan speed 7.32 μm/s. The scan speed of (b) and (c) are very high speed 732 μm/s. (a) and (b) are controlled feedback only. (c) is suppressed the error by STLO. From these results, STLO can suppress the tracking error at high-speed scanning.

ACKNOWLEDGMENT

The authors would lile to note that part of this research is supported by the Grant-ib-Aid for Young Scientists (A) from the MEXT of Japan (18686036, 2068608).

REFERENCES

[1] D. Y. Abramovitch, S. B. Andersson, L. Y. Pao, and G. Schitter. "A Tutorial on the Mechanisms, Dynamics, and Control of Atomic Force Microscopes," *Proc. Amer. Ctrl. Conf.*, pp. 3488-3502, 2007.

[2] N. Kodera, H. Yamashita, and T. Ando, "Active damping of the scanner for high-speed atomic force microscopy," *Rev. Sci. Instrum.*, vol. 76, p. 053708, 2005.

[3] G. Schitter, A. Stemmer and F. Allgower, "Robust two-degree of-freedom control of an atomic force microscope," Asian Journal of Control, 6, 2, pp. 156-163, 2004.

[4] T. Uchihashi, N. Kodera, H. Itoh, H. Yamashita and T. Ando, "Feed-Forward Compensation for High-Speed Atomic Force Microscopy Imaging of Biomolecules," *JJAP*, vol. 45, No. 3B, pp. 1904-1908, 2006.

[5] T. Sulchek, R. Hsieh, J. D. Adams, G. G. Yaralioglu, S. C. Minne, C. F. Quate, J. P. Cleveland, A. Atalar, and D. M. Adderton, " Highspeed tapping mode imaging with active Q control for atomic force microscopy," *Applied Physics Letters,* vol. 76, p. 1473, 2000.

[6] S. Tien, Q. Zou, and S. Devasia, "Iterative Control of Dynamics-Coupling-Caused Errors in Piezo scanners During High-Speed AFM Operation," *IEEE Trans. Ctrl. Sys. Tech.*, vol. 13, no. 6, pp. 921-931, 2005.

[7] K.Aoki, H.Fujimoto, "Nano Scale Servo Control of Atomic Force Microscope Based on Surface Topography Observer," IIC-06-132, pp1-6, 2006. (in Japanese)

[8] T. shiraishi, H. Fujimoto, "Proposed of Surface Topography Observer for Tapping mode AFM," IIC-07-119, pp. 7-12, 2007. (in Japanese)

[9] T. Ohshima, H. Fujimoto, "Proposed of Surface Topography Learning Observer for Contact mode AFM," IIC-07-117, pp. 7-12, 2007. (in Japanese)

[10] A. Sebastian, M. V. Salapaka, D. J. Chen and J. P. Clevelamd, "Harmonic analysis based of tapping-mode AFM", *Proc. Amer. Ctrl. Conf.*, pp. 232-236, 1999.

[11] S. Salapaka, T. De, and A. Sebastian, "Sample-profile estimate for fast atomic force microscopy," Appl. Phys. Lett., vol. 87, p. 053112, 2005.

[12] Jeffrey A. Butterworth, Lucy Y. Pao, Daniel Y. Abramovitch, " Architectures for Tracking Control in Atomic Force Microscopes," in Proc. IFAC 17th World Congress, pp. 8236-8250, 2008.

[13] M.Tomizuka: "Zero Phase Error Tracking Algorithm for Digital Control", Trans. ASME, Jounal of Dynamic Systems, Measurement, and Control, Vol.109, pp.65-68 (1987)

[14] K. J. Åström and J. Sternby : "Zeros of sampled stetem", Automatica, vol. 20, no.1, pp. 31-38 (1984).